Journal of Colloid and Interface Science 657 (2024) 830–840

Contents lists available at ScienceDirect

Journal of Colloid And Interface Science

journal homepage: www.elsevier.com/locate/jcis

Regular Article

Deformation of confined liquid interfaces by inhomogeneous electric fields and localized particle forces

Faranaaz Rogier [a], Wan Shao [b,c], Yuanyuan Guo [b,c], Lei Zhuang [b,c], Willem K. Kegel [a], Jan Groenewold [a,*]

[a] Van 't Hoff Laboratory for Physical and Colloid Chemistry, Debye Institute for Nanomaterials Science, University Utrecht, Padualaan 8, Utrecht, 3584 CH, the Netherlands

[b] Guangdong Provincial Key Laboratory of Optical Information Materials and Technology & Institute of Electronic Paper Displays, South China Academy of Advanced Optoelectronics, South China Normal University, Guangzhou 510006, PR China

[c] National Center for International Research on Green Optoelectronics, South China Normal University, Guangzhou 510006, PR China

GRAPHICAL ABSTRACT

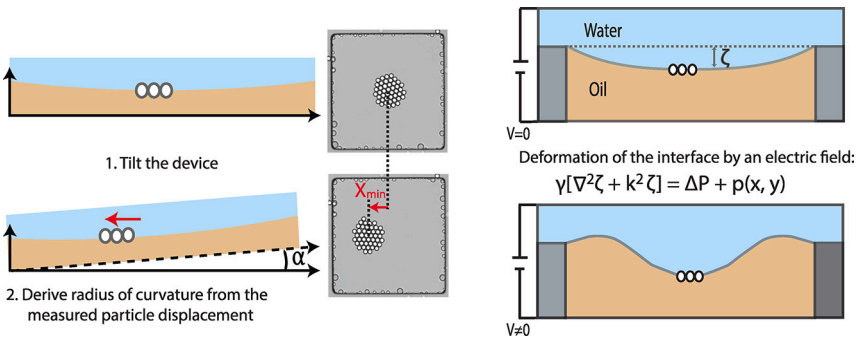

ARTICLE INFO

Keywords:
Capillarity
Electric fields
Interfacially adsorbed particle
Liquid-liquid interface
Electrowetting

ABSTRACT

Hypothesis: Oil-water interfaces that are created by confining a certain amount of oil in a square shaped pixel (~ 200 x 200 μm^2 with a height of ~ 10 μm) topped by a layer of water, have a curvature that depends on the amount of oil that happens to be present in the confining area. Under the application of an electric field normal to the interface, the interface will deform due to inhomogeneities in the electric field. These inhomogeneities are expected to arise from the initial curvature of the meniscus, from fringe fields that emerge at the confining pixel walls and, if applicable, from interfacially adsorbed particles.

Modeling and Experiments: We model the shape of the confined oil-water interface invoking capillarity and electrostatics. Furthermore, we measure the initial curvature by tracking the position of interfacially adsorbed particles depending on sample tilt.

Findings: We found that the pixels exhibited meniscus curvature radii ranging from 0.6-7 mm. The corresponding model based minimum oil film thicknesses range between 0.7 and 9 μm. Furthermore, the model shows that the initial meniscus curvature can increase up to 76 percent relative to the initial curvature by the electric field

* Corresponding author.
E-mail addresses: f.rogier@uu.nl (F. Rogier), w.k.kegel@uu.nl (W.K. Kegel), j.groenewold@uu.nl (J. Groenewold).

https://doi.org/10.1016/j.jcis.2023.11.099
Received 28 April 2023; Received in revised form 13 November 2023; Accepted 16 November 2023
Available online 6 December 2023

before the oil film becomes unstable. The pixel wall and particles are shown to have minimal impact on the interface deformation.

1. Introduction

There is significant interest in the behavior of interfacially adsorbed particles, with research ranging from contact angle measurements [1], adsorption behavior [2,3], capillary forces [4–6] and electrostatic interaction caused by the surface charge of the particles [7–9]. Even though electric fields may facilitate colloidal assembly [10], experimental studies on electrically induced interactions of colloids at interfaces are limited [11,12]. In order to study electric field induced forces on colloidal particles adsorbed on a liquid-liquid interface, there is a challenge to provide a stable liquid and a stable interface. A common problem that occurs in experiments with large electric fields and oil-water interfaces, is uncontrolled flow of the liquid and electrode reactions [13]. In the available studies, the experiments are limited to large particles and oil-oil interfaces [11,12]. To solve these issues, our research turned to the use of electrowetting pixels. These pixels are based on two phase liquid-liquid flows driven by an electric field. In this paper we aim to characterize the deformation of the oil-water interface in these pixels, where we consider the effect of the initial curvature of the liquid interface, the pixel wall and particles that are adsorbed on the interface.

Even though liquid-liquid interface deformations have been studied for electrowetting purposes [14,15], many studies are merely focused on the rupture of the interface [16,17] or the movement of the contact line [18,19]. These studies are not suitable to study particle interaction, since large deformations and the rupture of the interface interfere with the particle interaction. In this research we focus on characterizing interface deformations that occur below the rupture voltages. The deformation of the meniscus of a pendant droplet at the end of a capillary tube is studied in [20], here it was found that curvature is enhanced by an electric field.

The pixels in this paper are produced in two dimensional arrays of pixelated foils and are used in prototypes for electrowetting displays [21]. An electrowetting pixel typically consists of a square area of superhydrophobic surface which is enclosed by walls, see Fig. 1. An oil film is confined in the pixel by capillary forces due to the pixel wall. The oil film is topped with a layer of water. This system is enclosed between two electrodes parallel to the oil-water interface such that an electric field can be applied across the liquids. As depicted in Fig. 1, one can see that the contact line is envisaged to be pinned to the edge of the pixel wall.

There are several advantages of using an electrowetting pixel in the context of studying colloidal particles under the application of an electric field. The first advantage is that, by design, a negligible amount of electrochemical degradation is expected. In addition, due to the strong capillary confinement and limited height of the liquid films, it is unlikely that electro-hydrodynamic instabilities will occur. Another advantage is that the pixelated foil can generate a large amount of data, since every pixel can be studied separately. For example, experimental designs where the number of particles is different for each pixel enables to perform parametric studies in a natural way. At high voltage, above the so called rupture voltage, it is known that the oil film in the pixel ruptures, see [22]. In this study the applied voltage is well below the rupture voltage. To minimize shielding effects of charge carriers that are present in the water and oil phases, see Ref. [23], we resort in this study to the use of AC-driving instead of DC driving which is customary for the display application.

A peculiarity of such pixels is that the oil-water interface generally is not flat but is expected to be slightly curved due to incomplete filling with oil of the pixel. In the standard capillary filling process of a pixelated foil [21], the amount of oil trapped varies from pixel to pixel [24] but is generally insufficient to form a flat interface. As a result, the shape of the oil meniscus is concave, as depicted in Fig. 1. The interface shape may vary from flat up to having a curvature such that the center almost touches the bottom surface. This curvature of the oil-water interface has an impact on the forces acting on the colloidal particle. For example, when particles have a higher density than the fluid, the particle position will be biased towards the center of the pixel due to the effective gravitational pull on the particle. To correctly interpret the particle behavior in such pixels, it is thus of interest to quantify the amount of underfilling. Also, a non-zero initial curvature implies that the oil film thickness varies as a function of lateral position. The oil thickness is minimal in the pixel center and becomes larger towards the pixel walls. The oil thickness is an important factor that determines the electric field strength in the oil film. The curvature therefore leads to the electric field being highest in the pixel center and gradually becoming weaker as one moves towards the pixel wall. This in turn impacts the polarization of particles that may be present on the oil water interface. Another effect of the uneven distribution of electrostatic pressure acting on the oil-water interface is that it tends to amplify the initial curvature. A similar effect was described by the deformation of a droplet suspended in a fluid and exposed to an electric field, in references [25,26].

As discussed above quantifying the oil-water curvature is desirable, therefore a method is presented to measure the curvature of the liquid-liquid interface by following the particle position as a function of tilting the sample. The theoretical part of this work is a calculation of the effect of electric field on the curvature of the oil-water interface. This model describes the interplay between electrostatic, capillary, and gravitational forces, and how it determines the shape of the meniscus. Quantifying this effect opens the way to measure the interaction potential between adsorbed particles which will be the topic of forthcoming work. In addition, the manipulation of liquid-liquid curvature is of interest in the context of electrically tuneable lenses [27,28].

This paper is organized as follows. In section 3 the above-mentioned method to measure the initial interfacial curvature by means of sample tilting is described and applied. Subsequently, the effect of electric field on curvature as it depends on underfilling is explored theoretically in section 5.1. The initial curvature is not the only factor that determines the shape of the meniscus at a specific electric field. In particular, the pixel wall can be expected to have an effect on interface shape. Since the pixel wall material typically has a higher dielectric constant compared to oil, it distorts the electric field in its vicinity. The effect of this electric field distortion, referred to as the fringe field, is determined for an exponentially decaying fringe field with general prefactor and decay length in section 5.2. With the aid of a simulation using COMSOL the exponential decay of the fringe-field has been confirmed for typical pixel dimensions and both the decay-length and prefactor have been established for a typical pixel. Then, by combining the simulation result with the calculated effect of fringe fields on interface shape, the effect of the pixel walls on the curvature can be estimated. The last factor that we discuss to influence the curvature of the interface is the presence of adsorbed particles that exert localized forces normal to the interface. The effect of these forces on the effective curvature is being treated in section 5.3.

2. Materials and methods

2.1. Electrofluidic device

The unfilled electrowetting devices were prepared as in reference [22]. The ITO (Indium tin oxide) was coated with an amorphous fluoropolymer (AF1600, Chemours, $\epsilon_{dl} = 1.934$, thickness $h_{dl} \approx 0.85$ μm) and forms a dielectric layer. The insulator was spin-coated on ITO/glass

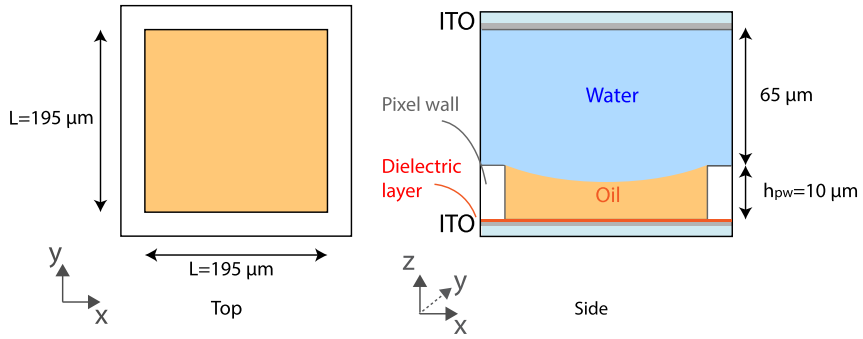

Fig. 1. Schematic representation of the electric cell. On the left panel a top view is shown and on the right a side view. The top view shows the lateral enclosure of the oil film by square shaped pixel walls. The side view depicts the oil film topped by the water layer and sandwiched between two parallel planar transparent ITO electrodes. In the side view one can see how the contact line to coincides with the pixel wall corner. It will be assumed that the contact line remains pinned to this position.

substrates, which has a resistivity of 100 ΩSq. The pixel walls were formed from an n-type photoresist (SU8-3005, Microchem) by lithography. The pixel wall form square shaped compartments and have a height of $h_{pw} = 10$ µm, as is schematically depicted in Fig. 1.

The oil is deposited on the bottom ITO-coated and pixelated glass slide by dispensing an oil droplet on the edge. Then, the droplet is carefully pushed over the glass slide by a thin plastic sheet in a sweeping motion. The suspension of MilliQ water with silica particle (*Microparticle GmbH*, radius of 3.75 µm) is added on top of the oil. The device is closed with an ITO glass slide on top and secured with pressure sensitive adhesive and UV-glue on the edges. To ensure that all particles are adsorbed on the interface, the device is placed upside down of several minutes. This causes the particles that did not adsorb on the interface to sediment towards the ITO glass slide and stick irreversibly.

2.2. Tilting experiment

The electrowetting device was placed on the microscope (Nikon Ti-e) with a LED light-source (*CoolLED pE-100*) and camera (*The Imaging Source*). The microscope was tilted by lifting the front while leaving the electrofluidic device at its position on the microscope. By careful alignment of the electrowetting device on the microscope, the device is tilted in the direction towards a side of the square pixel, for example in the y-direction. Slight deviations in the x-direction can be corrected while observing the displacement of the cluster in the pixel, such that a displacement in the x-direction is negligible. The tilting angle was calculated from the measured tilting height, at a width of 56.2 cm. Approximately 5 tilting heights were chosen to determine the curvature, these heights could range between 0 and 20 mm. The uncertainty in the tilting angle is 0.1° and originates from the uncertainty in the measured width and height. The curvature of the interface is not known a priori, therefore the binsize and the range of the heights were adapted according to the observed displacement of the particles during the tilting experiment. The displacement of the center of the mass of the particles were measured as is described in the following section.

2.3. Center of mass tracking

The images where aligned in Fiji, with the plug-in 'Template Matching' to correct for small displacements of the device during recording an imaging sequence that could have occurred by the device sliding and shifting on the microscope glass-holder. A pixel wall was used as a reference for the template matching. To track the particles, a pixel was cropped to the region of interest. A threshold was applied to the images to remove background noise. Depending on the quality of the image, appropriate image processing steps were used, such as a bandpass filter, the method 'Fill holes' and a Gaussian blur, which would leave the center of mass unaffected. These processing methods were used as provided by Matlab or FIJI.

After applying the threshold, all particles in a cluster consisting of n black-colored pixels in a frame that is labeled t. $x_{i,t}$ is the x-coordinate of the ith pixel in frame t and $y_{i,t}$ is the y-coordinate of the ith pixel in frame t. The coordinates of the averaged center of mass of cluster (X, Y) are measured by averaging over all the x- and y-coordinates respectively and all the frames T of the recording.

$$X = \frac{1}{T}\frac{1}{n}\sum_{t=1}^{T}\sum_{i=1}^{n} x_{i,t} \tag{1}$$

$$Y = \frac{1}{T}\frac{1}{n}\sum_{t=1}^{T}\sum_{i=1}^{n} y_{i,t} \tag{2}$$

3. Experimental determination of the curvature

By adding a fluorescent dye to the oil it is observed that the fluorescent intensity in the pixel varies with lateral position, being strongest in the pixel center. This is indicative of a non-uniform oil thickness within the pixel, details of which are given in the SI. As already discussed, due to the meniscus pinning at the pixel wall in combination with an underfilling by oil, a curved meniscus is expected. The amount of oil in a pixel determines the curvature. Since the behavior of the particles is strongly determined by the curvature of the interface, the tilting-method was developed to accurately measure the curvature of every pixel. Another example of tilting samples that contain colloids has been employed in [29]. In that work, the areal density of colloids is manipulated by sample tilting and as such the equation of state is being investigated.

Since the pixels are square shaped, the interface is not perfectly spherical as one would expect for an interface confined by a circular pixel wall. Still, sufficiently close to the center of the pixel, the interface shape will be approximately spherical. Further, within the approximation of small slopes the interface shape can be considered as parabolic. To avoid confusion, 'curvature' is always referred to the curvature in or close to the center of the pixel. In addition, the curvature in the absence of an electric field is referred to as initial curvature. So the initial curvature is the curvature that arises from the incomplete filling as has been described in the introduction. The initial curvature can be quantified by adding particles that adsorb onto the interface and measure the shift in their equilibrium position upon slightly tilting the pixel. In what follows, the relation between tilt and curvature will be derived theoretically. Around the center of a pixel, where the deformation by the walls can be neglected, the interface has approximately a parabolic shape:

$$\zeta(r) - \zeta_c \approx \frac{r^2}{2R} \tag{3}$$

Here, R is the radius of the curvature and r is the radial distance from the center of the pixel. Further $\zeta(r)$ is the z position of the oil-water interface and ζ_c its value in the center of the pixel. See Fig. 4 for a graphical depiction of the coordinates.

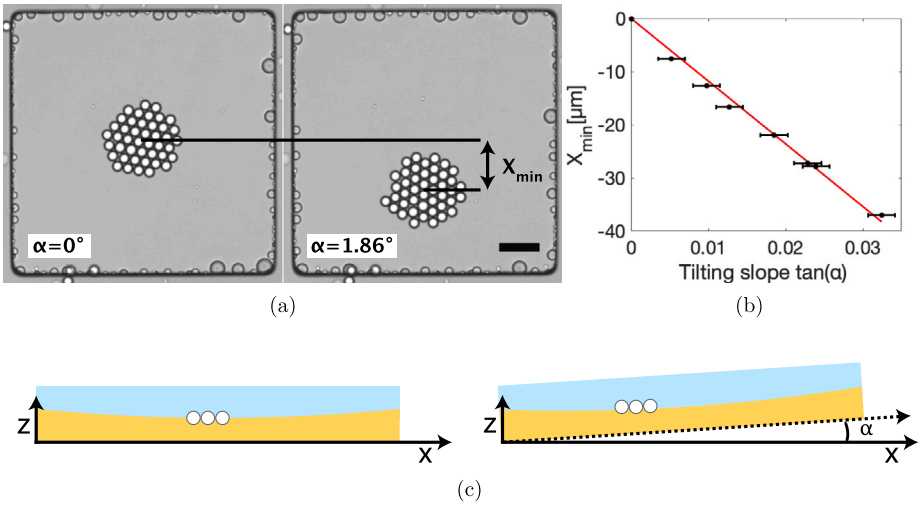

Fig. 2. a) Microscope image of a pixel containing interfacially adsorbed particles tilted with an angle $\alpha = 1.86°$. The deviation from the central position Δx is tracked and plotted versus the tilting angle α, the result of which is shown in panel b) Here, the radius of curvature found from the fit is $R = 1.18 \pm 0.05\, mm$. Scalebar = 30 μm. c) Is a graphical depiction of how the shift in equilibrium position of the pack of particles shifts as a result of the tilting.

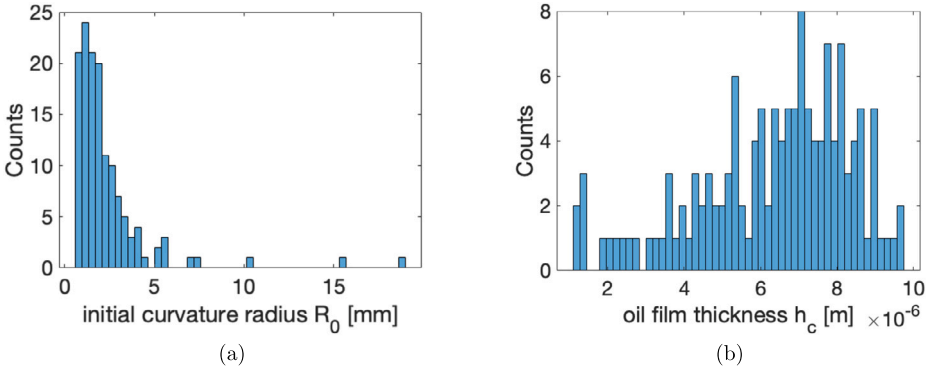

Fig. 3. a) Statistical distribution of curvature radii as measured by the tilting method for 137 randomly selected pixels; b) Statistical distribution of the corresponding central oil film thicknesses corresponding to the curvature radii in panel a.

To measure the displacement of the particle, the x-axis is chosen to be in the tilting-direction with α the tilting angle, as shown in Fig. 2c. The lateral position of the average center of mass of a particle or of a pack of particles will be denoted by (X, Y). Here, the average center of mass is the averaged x- and y-coordinate in time and over all particles in the cluster, as is explained in the material section. For particle positions capital letters are used and these are measured with respect to the pixel center. Here it is assumed that the tilt is in the x-direction. The z-position of the particle can be assumed to follow the z-position of the meniscus in the laboratory frame:

$$\zeta_{tilt}(X) - \zeta_{tilt}(0) = \frac{X^2}{2R} + X \tan\alpha \tag{4}$$

In Eq. (4) the lift of the particle in the laboratory frame with respect to the pixel center is expressed as the result of curvature plus the effect of tilting the interface. Here it is assumed that the particle moves along the line where $Y = 0$. The lateral position of the particle corresponding to the position of minimum gravitational energy is denoted by X_{min}, and is found by minimizing the particle height in the laboratory frame: $\left|\frac{\partial \zeta_{tilt}}{\partial X}\right|_{X_{min}} = 0$. This results in the following relation between equilibrium position of the particle and the tilt angle:

$$X_{min} = -R \tan\alpha \tag{5}$$

From Eq. (5) it follows that the meniscus curvature of a pixel can be obtained by systematically tilting the sample. Specifically, the radius of curvature R can be determined by measuring the displacement X_{min} for different angles α. Fig. 2a show a bright field microscope image at different tilting angles, where the clusters of particles move X_{min} from the center position for a tilt of $\alpha = 1.86°$. The shift of the averaged center of mass relative to the center position is measured and plotted for each angle α. Fig. 2b shows the corresponding X_{min} plotted against the tilting slope and the linear fit.

This method is applied to a sample of pixels to show the variability in meniscus curvature and corresponding central oil film thickness. A random selection of 137 pixels in our particle laden pixelated foil was analyzed as a function of tilt angle. For each of these pixels the initial radius of curvature was determined, the results of which are plotted in a histogram shown in Fig. 3a. The histogram shows that most pixels have an interface with a radius of curvature ranging from 0.6-7 mm. Due to underfilling the thickness of the oil film is expected to be reduced. This reduction will be larger as the curvature becomes larger. In section 4 a model is presented with which the relation between curvature and thickness of the oil film in the pixel center is calculated, see paragraph 5.1. The histogram of central oil film thickness corresponding to the measured curvatures is shown in Fig. 3b.

It is not surprising to find such a variability in meniscus curvature given the manual filling of the pixels. In the context of display manufacturing novel techniques of pixel filling employing inkjet [30] are being exploited in order to reduce the variability in meniscus curvature. Based on the variation in oil film thickness near the center, the electric field at that position is expected to vary substantially per pixel. It is of importance to quantify the effect of filling on electric field to

better interpret studies on interfacially adsorbed particles in such pixels. As mentioned, this variation in curvature by uncontrolled filling is undesirable from a technological point of view. However, from an experimental point of view this variation can be exploited. For instance by systematically investigating the effect of curvature on interfacially adsorbed particles. The large variety of curvatures that emerge from the filling process enables to screen many different curvatures within a single pixelated foil.

4. Model for the meniscus shape

As discussed, it is of importance to have knowledge of the meniscus shape. For instance an accurate prediction of the value of the electric field in the pixel center depends on the precise shape of the meniscus. In addition, the curvature in the center plays an important role in the behavior of interfacially adsorbed particles added to the pixels. For this reason a model is developed that enables to predict the shape of the meniscus under the influence of an electric field in a typical pixel.

The model used here to calculate the meniscus shape is derived from considering the total free energy of the system as a functional of the interface shape. The approach presented here follows the one outlined in references [22] and [31]. The free energy functional comprises capillary, electrostatic and gravitational contributions. It will be shown that the gravitational contribution can be neglected. To obtain an equation for the meniscus shape, the free energy functional is minimized with respect to variations in the interface position while respecting a mass conservation constraint.

4.1. Characteristics and assumptions of the system

For a depiction of the pixel geometry and definition of geometric variables see Fig. 1. The parallel planar ITO electrodes have their normal vector oriented in the z direction. The typical dimensions of a pixel are a few hundred microns wide and tens of microns thick. In Fig. 1, the dimensions of the pixel used in the experiments are denoted. The oil film thickness, h_{pw} is typically a few microns. As a result, the slope of the meniscus with respect to the electrode direction will typically be a few micrometers over several hundred micrometers (≈ 0.01). Therefore, it is reasonable to assume that the electric field in the liquids will be predominately in the direction normal to the electrode. The z-component of the electric field near the interface and in the oil, E, will be nearly equal to the component normal to the interface for a curved interface and the tangential components in the electrostatic energy can be neglected.

On the level of the pixel, capillary forces are more dominant compared to gravitational forces. This is reflected by a capillary length $\lambda_C = (\gamma/\Delta\rho g)^{1/2}$ that exceeds the dimensions of the pixel. For density differences $\Delta\rho$ of 200 kg/m^3 that are typical for oil-water systems and an interfacial tension of $\gamma 0.051$ J/m^2 one finds a value for λ_C of 5 mm. The pixel size L ranges typically from 100 to 300 μm. Therefore, the Bond number on the pixel scale $Bo = L^2/\lambda_C^2 < 0.01$, is much smaller than unity. This condition means that the capillary forces are sufficiently strong to keep the oil from flowing out of the pixel due to the weight of the overlaying water layer.

The effect of the applied voltage is that electrostatic forces are generated. The dimensionless number $\epsilon E^2 L^2/h_{pw}\gamma$, with ϵ the dielectric constant of the liquid, exceeds unity if on the pixel scale these dielectric forces are larger than the capillary forces. This is a similar condition to the requirement that the applied voltage is lower than the rupture voltage. On the scale of a particle or cluster of particles with radius a the dielectric versus capillary force balance is expressed by: $\epsilon E^2 a/\gamma$. This dimensionless number is also much smaller than unity for micron sized particles, which means that the changes in meniscus curvature due to the presence of the particle will be small.

If the rupture voltage is reached, the capillary forces and electrostatic forces are in balance. It has also been established that the Bond number is small. Therefore, if below the rupture voltage gravitational forces can be safely neglected.

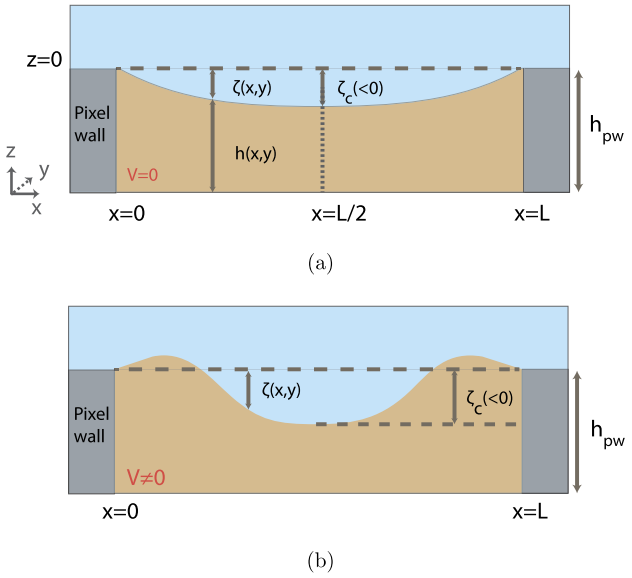

Fig. 4. Schematic depiction of the meniscus shape in the pixel indicating the definition of the geometric variables for a) in absence of applied electric field b) in presence of electric field.

4.2. Model

The oil-water interface will be described with a position in the normal direction (z-direction) as a function of the two lateral coordinates (x, y), see Fig. 4. The position of the oil-water interface $\zeta(x, y)$ is given by the distance in the normal direction between the oil-water interface position and the top of the pixel wall as a function of the lateral coordinates. This interface position can be expressed as follows:

$$\zeta(x, y) = h(x, y) - h_{pw} \tag{6}$$

Where $h(x, y)$ is the oil film thickness as a function of the position in the pixel and h_{pw} is the height of the pixel wall. The meniscus is assumed to be pinned at the edges of the pixel wall that encloses the pixel with a square shape. As such the oil film thickness at the pixel wall should be equal to h_{pw}. With the coordinate system chosen here, the position of pixel wall is at the lateral locations $x = 0$, $x = L$, $y = 0$ and $y = L$, see Fig. 4. Consistent with Eq. (6) it is imposed that $\zeta = 0$ at these locations, thus expressing the assumption of contact line pinning.

To model the meniscus shape and its response to an externally applied electric field, the following free energy contributions are considered: capillary, electrostatic and gravitational. First, one has the capillary free energy. A change in meniscus shape will generally change the total area of the oil-water interface. Multiplying the change in area with the interfacial tension of the oil-water interface γ gives the free energy changes with respect to a flat interface:

$$\Delta G_{cap} \simeq \frac{1}{2}\gamma \int_0^L \int_0^L |\nabla\zeta(x, y)|^2 dx dy \tag{7}$$

Here, ∇ is the 2-dimensional gradient operator. This expression for the energy becomes is accurate for slopes $|\nabla\zeta(x, y)| << 1$, which is assumed to be the case here.

When an external electric field is applied across a pixel via the ITO electrodes as depicted in Fig. 1, the electrostatic energy of the system is described by:

$$\Delta G_{es} \simeq -\frac{1}{2}V^2 \int_0^L \int_0^L \left(c[h(x,y)] - c[h_{pw}]\right) dx\, dy$$

$$= -\frac{1}{2}V^2 c'[h_{pw}] \int_0^L \int_0^L \zeta(x,y) dx\, dy$$

$$- \frac{1}{4}V^2 c''[h_{pw}] \int_0^L \int_0^L |\zeta(x,y)|^2 dx\, dy + \ldots \quad (8)$$

Here, $c[h]^{-1} = h_{oil}/\epsilon_{oil} + h_w/\epsilon_w + h_{dl}/\epsilon_{dl}$ is the capacitance per unit area, of a system with a uniform oil film thickness h_{oil}, a water layer thickness h_w, a dielectric layer thickness h_{dl}, and with the externally applied voltage V. Then, $\epsilon_{dl}, \epsilon_{oil}$ and ϵ_w are the dielectric constants in SI units of the dielectric layer, the oil film and the water layer respectively. $c'[h]$ and $c''[h]$ are the first and second derivatives with respect to the oil film thickness of the capacitance per unit area. In the case of AC driving, this voltage has an effective value after time averaging, the so called V_{rms}. The expression (8) is approximate as it ignores contributions to the electrostatic free energy related to components of the electric field parallel to the oil water interface. These components arise when the interface is not flat, but can be neglected as long as the slope of the interface is small. The function is expanded in ζ up to quadratic order. The first term is linear in $\zeta(x,y)$ and is comparable to the linear term of the gravitational energy. The total free energy is $\Delta G = \Delta G_{cap} + \Delta G_{es} + \Delta P_0 \int_0^L \int_0^L \zeta(x,y)$. It is the sum of the capillary (Eq. (7)) and electrostatic (Eq. (8)) energy. Moreover, it includes a hydrostatic pressure term $\Delta P_0 \int_0^L \int_0^L \zeta(x,y)$ that serves to ensure that the total amount of oil is fixed. The total free energy is now written as:

$$\Delta G \simeq \frac{1}{2}\gamma \int_0^L \int_0^L [|\nabla\zeta|^2 + k^2\zeta^2] dx\, dy + \Delta P \int_0^L \int_0^L \zeta(x,y) \quad (9)$$

With the characteristic wavenumber:

$$k^2 = \frac{V^2 c''[h_{pw}]}{2\gamma} \quad (10)$$

Moreover, the linear terms are collected into an effective pressure difference $\Delta P = \Delta P_0 - \frac{1}{2}V^2 c'[h_{pw}] + g h_{pw} \Delta\rho$ which also includes the hydrostatic pressure ΔP_0.

In case of a flat interface this free energy has already been subject to analysis in [22]. From this work it is known that for critical values of the characteristic wavenumber, the meniscus becomes unstable. The oil film will rupture for voltages that are high enough such that the critical wavenumber is exceeded. The voltage corresponding to this critical value is called the rupture voltage and notated as V_c. In the SI, a ruptured interface is shown and described in more detail.

New compared to the previous work in this context [22] and [31] is the initial state of the interface which in the case here has a nonzero curvature. This initial curvature is being incorporated by imposing a hydrostatic pressure. Another novelty is the inhomogeneous nature of the electrostatic force on the interface.

To proceed consider the downward force per unit area on the meniscus which is obtained by taking the functional derivative of the total free energy with respect to the meniscus shape: $\frac{\delta G}{\delta \zeta} = -\gamma[\nabla^2\zeta + k^2\zeta] + \Delta P$. In equilibrium there should be no net force anywhere on the oil-water interface. This leads to the following equation that describes the meniscus shape in the presence of gravity and electric field:

$$\gamma[\nabla^2\zeta + k^2\zeta] = \Delta P \quad (11)$$

with ΔP the pressure difference between the oil and water phase which must be independent of position. This pressure difference should have a value such that the following condition holds:

$$\int_0^L \int_0^L \zeta(x,y) dx dy = L^2 \bar{\zeta} \quad (12)$$

where the average underfilling, denoted by $\bar{\zeta}$, should be considered fixed. This condition is derived from the assumption that the total amount of oil in the pixel is fixed and can be considered incompressible. For a perfectly filled pixel, the total volume of oil is $L^2 h_{pw}$. The average underfilling in this case is $\bar{\zeta} = 0$. The effective pressure difference ΔP can be used as a Lagrange multiplier to determine the degree of under filling.

Additional forces, such as the fringe fields due a pixel wall or the presence of particles, will add a positional dependent pressure $p(x,y)$ to the right hand side of Eq. (11) and is to be considered small compared to the overall effective pressure difference. The meniscus shape equation then has the form:

$$\gamma[\nabla^2\zeta + k^2\zeta] = \Delta P + p(x,y) \quad (13)$$

The shape equation, along with the boundary conditions in equation (12) can be solved by using Fourier transformations as detailed in the SI.

5. Model results

5.1. Effect of underfilling

Near the center of the pixel, the curvature is, to a good approximation, described by Eq. (3). The radius of curvature R and ζ_c, which is the central deviation of the film thickness from h_{pw}, are functions of the applied electric field and the amount of underfilling.

The underfilling of the pixels will be characterized by the initial radius of curvature in absence of an electric field, R_0:

$$\frac{1}{R_0} \simeq -C\frac{\zeta_c(V=0)}{L^2} \quad (14)$$

The proportionality constant is given by: $C \simeq 6.81$ and is found by numerically implementing the theory presented in section 4 via a Fourier transformation technique. Details about the numerical procedure are given in the SI. Depending on the initial curvature, the electric response of the meniscus is also calculated by the model. An example of how the meniscus shape changes due to the electric field is shown in Fig. 5. The numerical results of the curvature response can be summarized as follows:

$$\frac{1}{R} = \frac{1}{R_0} + \beta\frac{1}{R_0}\left(\frac{V}{V_c}\right)^2 + \ldots \quad (15)$$

The constant β determines the response of the curvature to the electric field. For the pixel dimensions and materials used here, it is found that $\beta = 0.76$, as determined by numerical analysis, see SI. As long as the Bond number is small (see section 4.1) and the voltage is well below the rupture voltage, the results of Eq. (14) and (16) are independent of the pixel dimensions.

5.2. Effect of the pixel wall

The pixel wall has a different dielectric constant from both oil and water. This causes lateral inhomogeneities in the electric field near the pixel walls, even for an initially flat interface. These deviations in the electric field are referred to as fringe fields and lead to an effective pressure gradient on the oil-water interface adjacent to the pixel wall. This will impact the meniscus shape according to Eq. (13). In this case, the excess pressure $p(x,y)$ is caused by the fringe fields.

To asses the effect of the pixel wall on the meniscus shape, the fringe pressure is assumed to be well represented by an exponential function depending on the distance to wall with a decay length ξ:

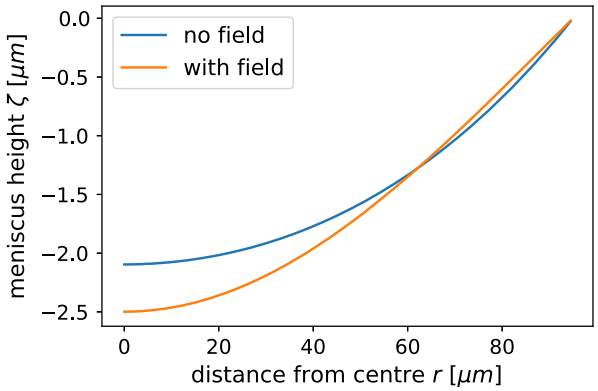

Fig. 5. Model results for the underfilling with and without electric field. The electric field corresponds to a voltage that is about fifty percent of the rupture voltage. The figure clearly shows the effect of the electric field to increase the initial curvature. (For interpretation of the colors in the figure(s), the reader is referred to the web version of this article.)

$$p(x,y) = P_{fringe}\left(\frac{V}{V_c}\right)^2\left[e^{-x/\xi} + e^{-(L-x)/\xi} + e^{-y/\xi} + e^{-(L-y)/\xi}\right] \tag{16}$$

The effect of the fringe fields can be added to the effect of initial curvature due to the linear form of Eq. (13) provided that the fringe pressure is independent of the initial curvature. Strictly speaking the fringe pressure is expected to be weakly dependent on the initial curvature. This effect will be neglected.

From simulations of the electric field in the pixel geometry it has been verified that this exponential form is a good representation of the fringe pressure. The simulation details can be found in the SI. From the same simulation we obtain the prefactor P_{fringe} and decay length ξ. The fringe pressure is found to be positive, which means that the oil film is effectively lifted in the vicinity of the pixel wall. This can be understood as follows. The electric field lines in the pixel wall material are more concentrated due to the higher dielectric constant compared to the oil. As a result, the concentration of field lines in the adjacent oil must be lower than average. The lower electric field near the wall means that the electrostatic pressure gradient is such that the electrostatic pressure in the center of the pixel is higher than near the wall, which amounts to an effective pull on the oil near the wall. In the opposite case, where the dielectric constant of the wall material would be lower compared to the oil, a push on the oil film in the vicinity of the wall is expected.

For an initially flat surface, the curvature induced by the fringe fields is expected to scale by the form:

$$\frac{1}{R} = -\kappa_{fringe}(\xi/L)\frac{P_{fringe}}{\gamma}\frac{\xi^2}{L^2}\left(\frac{V}{V_c}\right)^2 \tag{17}$$

This scaling form is based on dimensional analysis, which is based on the assumption that the only relevant length scales in the problem are the pixel dimension L and the decay length ξ and that the response of the curvature is linear in the fringe pressure prefactor P_{fringe}. The scaling function κ_{fringe} depends solely on the ratio of ξ and L. κ_{fringe} is determined numerically (see SI) and the results are shown in Fig. 6. Typical values for $\frac{\xi}{L}$ of fabricated pixels are between 0.05 and 0.2, see SI. Fig. 6 shows that within these values, κ_{fringe} varies considerably within this range of $\frac{\xi}{L}$. Due to the linear nature of the governing shape equation (13), the effect of fringe fields as expressed by Eq. (17) comes in addition to the effect of initial curvature expressed by Eq. (15).

The influence of the fringe field on curvature is expected to be negligible for the experimental pixel of choice. In Eq. (16), the decay length from the wall, ξ, and the prefactor is P_{fringe} of the fringe pressure are the relevant parameters assumed to describe the fringe effect. With a finite element simulation (COMSOL) it was found that $\xi = 23$ μm for the experimental pixel of choice (see the SI). As can be seen from Fig. 4 in the SI, the result of the simulation shows that in

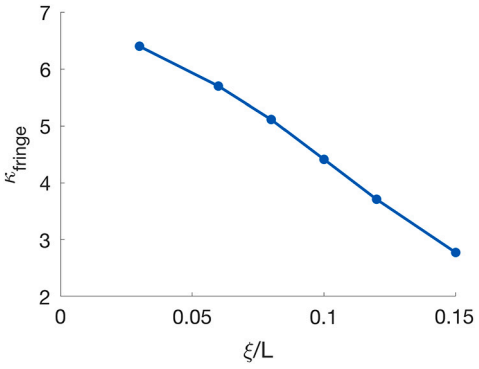

Fig. 6. Here the numerical determination of the scaling function that describes the effect of the fringe fields is shown. Definition of this function is shown in Eq. (17). The details of the numerical method are found in the SI.

the first 60 μm, the pressure decays exponentially as has been assumed in Eq. (16). To assess the effect of the fringe field on curvature the result Eq. (17) can be used. For the pixel size that has been used to carry out studies with interfacially adsorbed particles, one finds by COMSOL simulation that: $\frac{\xi}{L} = 0.11$, $P_{fringe} = -0.23$ Pa, $\gamma = 0.022$ J/m^2, leads to $1/R = 1/R_0 + 0.53(V/V_c)^2$, with R and R_0 in meters. This shows that the field dependent term is expected to be dwarfed by the term from underfilling, since the typical values for the initial radius of curvature are in the mm range. From this the term $1/R_0$ would be typically 3 orders of magnitude larger compared to the field dependent term. Therefore, for this type of pixels, the fringe fields give a negligible effect on the meniscus curvature.

5.3. Particle effect on curvature

As has been pointed out in the introduction, a possible follow up of this work is to study the interactions and force fields that interfacially adsorbed particles will experience if these are introduced in the pixels. It is anticipated that the gravitational forces that act on the particles will be relevant in the force balance acting on the particles. As seen in 3 the curvature is the only relevant factor determining the gravitational force on a particle. Therefore, in order to correctly study the particle behavior, the impact of the particles themselves on the curvature should also be addressed. We will show with this analysis that, under the experimental conditions of interest, this effect is negligible.

To proceed with the analysis of the particle effect on curvature only forces perpendicular to the interface are considered to have an impact on the meniscus shape; A parallel component of the force on the meniscus is expected to cause a lateral displacement of the particle instead of a deformation of the meniscus. A normal force f exerted by the particle on the meniscus, is assumed to act on a region with size a. Further, it will be assumed that the particles are partly wetted by both the oil and the water. Such type of adsorbed particle is referred to as a Pickering particle. In that case a is typically the radius of the approximate circle that the contact line traces on the particle surface. The spatial extent a, of the force ensures the absence of singularities in the numerical calculation. To rephrase, in case a is approaching zero, meniscus shape begins to show singularities, since the pressure locally becomes infinite in that hypothetical situation.

In view of the above discussion, the effective pressure distribution by a particle that exerts a net force f at location $(x_0, y_0) = (L/2 + X, L/2 + Y)$ on the meniscus, is assumed to have the following shape:

$$p(x,y) = -\frac{f}{2\pi a^2}e^{\frac{(x-x_0)^2+(y-y_0)^2}{2a^2}} \tag{18}$$

Note that this definition contains a minus sign which emerges from the convention that the pressure in Eq. (13) is defined as a pressure exerted on the oil film. The distribution is chosen such that the integral

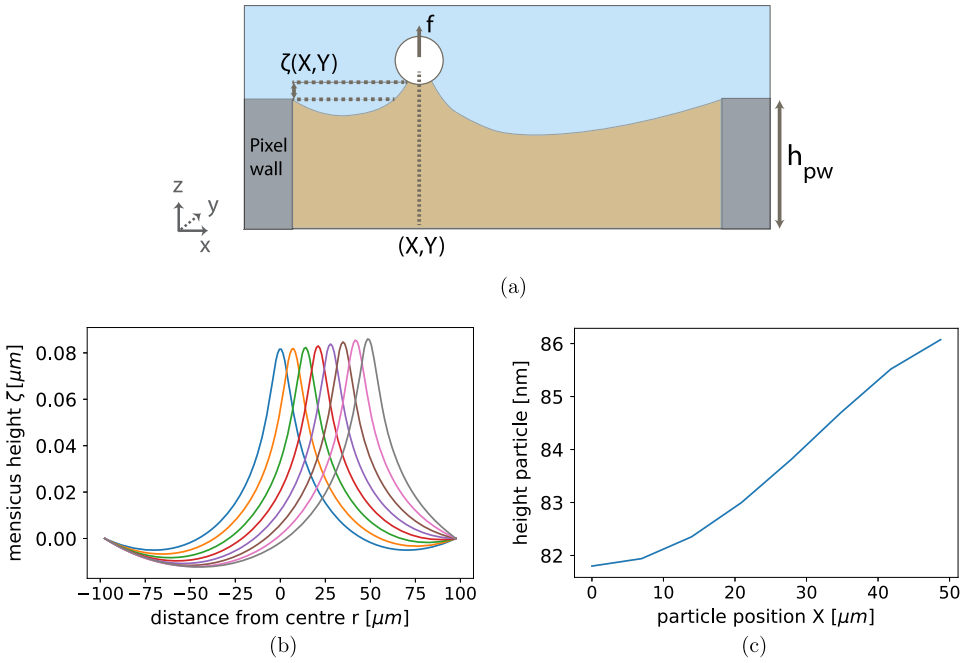

Fig. 7. a) Schematic depiction of the situation where a normal lift force acts on a interfacially adsorbed particle. b) Model results for a particle exerting a 5 nN lift force at varying lateral positions. c) Plot of the particle height as a function of lateral position as read from the results shown in panel b. It is seen that the particle height follows a different envelope compared to the unperturbed interface which in this case is chosen to be flat.

of the pressure over the entire interface results in the net force f. The particle force f is positive when it is directed in the positive z direction. For a positive f the particle pulls the oil film upwards. The pressure distribution assumed in equation (18) is arbitrary, but the conclusions are expected to be very similar for pressure distributions with a similar range and integrated force f.

This expression for pressure distribution exerted by a particle can be used in equation (13) to find the meniscus deformation that is caused by a localized particle force. In Fig. 7b the meniscus shape is plotted for a variety of particle positions. The quantity of interest is the curvature that a particle experiences, as it changes its lateral position. The meniscus height at the particle's location is determined numerically and is plotted in 7c. Denoting by $\zeta(X)$ the particle height as a function of the particle position, the curvature that the particle experiences is defined as:

$$\zeta(X) = \zeta_c + \frac{1}{2R}X^2 + \ldots \tag{19}$$

Here the particle height is traced by changing the X coordinate while keeping $Y = 0$. As stated, in Fig. 7b the particle height is plotted as a function of X. The particle height is described by a quadratic function of X for particle positions sufficiently close to the pixel center by Eq. (19). The curvature defined in Eq. (19) can be obtained numerically by fitting the result shown in Fig. 7b.

It is assumed that the capillary length is much larger than the system dimensions. The relevant scale for the long-range deformations of the meniscus is therefore the system size. Thus, the effect of a localized force on the curvature is governed by the system size. Moreover, it is expected that the curvature responds linearly to the applied force, since the shape equation is linear. With these considerations, the effect of a localized force on a confined meniscus is summarized into the following scaling form:

$$\frac{1}{R} = \frac{f}{\gamma L^2}\kappa_p\left(\frac{a}{L}\right) \tag{20}$$

For a collection of N particles, the force on the meniscus is assumed to be the number of particles multiplied by the force f and the force that the cluster of particles exerts on the meniscus is assumed to act on an area with radius $aN^{0.5}$. Equation (20) than generalizes to:

$$\frac{1}{R} = \frac{fN}{\gamma L^2}\kappa_p\left(\frac{aN^{0.5}}{L}\right) \tag{21}$$

In addition to the effective curvature, one also finds an effect on the meniscus height as a result of a particle in the center as defined in Eq. (19). This quantity, ζ_c, is captured in the following scaling equation:

$$\zeta_c = \frac{f}{\gamma}q_p\left(\frac{a}{L}\right) \tag{22}$$

Using the method to find meniscus shapes from the SI, the scaling functions q_p and κ_p can be obtained numerically. For a graphical representation of the numerical results for q_p and κ_p, see Fig. 8a and 8b respectively.

For $\frac{a}{L} < 0.1$, the scaling function q_p from Eq. (22) is well represented by a logarithmic function $q_p\left(\frac{a}{L}\right) \approx -0.157\ln\left(\frac{a}{L}\right) - 0.251$. The function that governs the radius of curvature is quite well approximated by a quadratic function of the ration a/L: $\kappa_p\left(\frac{a}{L}\right) \approx 1.01 - 8.35\frac{a}{L}^2$ for $\frac{a}{L} < 0.2$.

Similar to the effect of the fringe fields, the effect of particle forces on the experienced curvature is small. This can be illustrated by considering the gravitational forces exerted on the particle. The normal force on the meniscus exerted by the particle is $f = -mg$ where m is the negative of the buoyant mass. The lateral force is given by $f_{||} = -mgr/R$. Here r/R is the meniscus slope in the radial direction measured from the center and $1/R$ is the total curvature. The total curvature includes the initial curvature, the effect of the electric field on the curvature (eq. (15)), the curvature change due to the fringe field (eq. (17)) and the curvature change due to the particles themselves (eq. (21)). The effect of the normal particle force on the lateral particle force via the change in curvature is written as $\delta f_{||}$. With the aid of Eq. (21) this change in lateral particle force can be calculated as: $\delta f_{||} = f^2 r/\gamma L^2$, where $\kappa_p(a/L) = 1$ has been used. Inserting the values for a typical gives: $\delta f_{||}/f_{||} = mg/\gamma L \sim 2 \cdot 10^{-7}$. Here a particle buoyant mass of 10^{-13} kg has been used. This is a typical value for the buoyant mass of particle with several μm radius. As can be seen from the above the

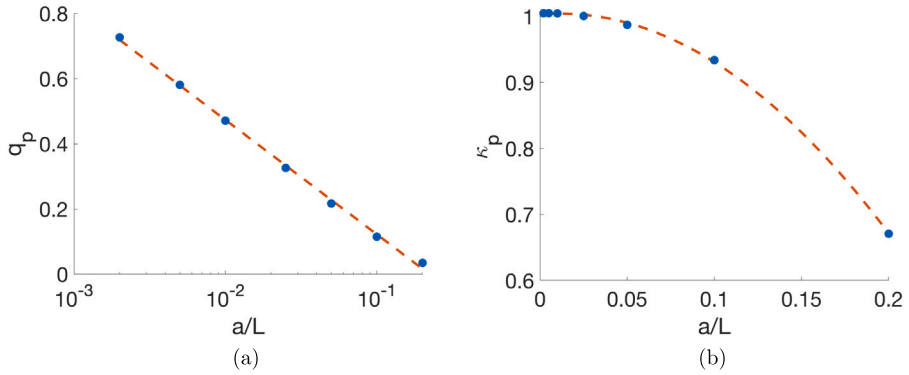

Fig. 8. Numerical results for the scaling functions that describe the influence of particle induced forces on the effective meniscus properties as a function of a/L where a is the effective support of the force distribution and L the pixel size. For definition of the scaling functions q_p describing the central meniscus position see Eq. (22). For the definition of the scaling function κ_p describing the curvature see Eq. (20).

effect of the particles themselves on the curvature is expected to be small. If the particle size is of order 100 μm or larger the effect of the particle itself on the meniscus curvature can no longer be ignored as the relative error scales with the particle buoyant mass.

6. Results and discussion

In section 5.1 the response of the curvature is shown as a result of the applied electric field according to a model for the meniscus shape under the influence electric field and capillarity. This same model is used to calculate the effect on the meniscus shape as a result of the fringe fields that stems from the pixel walls and the presence of particles that exert localized forces on the meniscus. To get the total effect on the curvature, the effect of particles, Eq. (21), should be added to that of fringe fields, Eq. (17) and underfilling, Eq. (15). This results in the following expression up to linear order in the particle force f and quadratic order in V:

$$\frac{1}{R} \simeq \frac{1}{R_0} + \left[\beta \frac{1}{R_0} + \kappa_{fringe}(\xi/L)\frac{P_{fringe}}{\gamma}\frac{\xi^2}{L^2}\right]\left(\frac{V}{V_c}\right)^2 + \frac{fN}{\gamma L^2}\kappa_p\left(\frac{aN^{0.5}}{L}\right) \tag{23}$$

In the preceding sections, the magnitude of these effects for typical pixel dimensions has been discussed. In particular it was found that for typical fringe fields and particles smaller than 100 μm, both the effect of fringe fields and particles on the meniscus curvature can be safely neglected. As a result the total curvature can be described by:

$$\frac{1}{R} \simeq \frac{1}{R_0} + \beta \frac{1}{R_0}\left(\frac{V}{V_c}\right)^2 \tag{24}$$

This relatively simple result is expected to enable the interpretation of experiments on particle laden pixels with relative ease. For instance the curvature experienced by the particles will be independent of the nature of the particles themselves. The initial curvature in the pixel close to the center is amplified by means of the applied electric field according to the calculations presented in section 5.1. To study the dielectrophoresis (see ref. [32]) and particle-particle interactions induced by applied electric fields (see ref. [33]), it is of importance to know the effect of electric field on the curvature. The curvature of the interface influences the interfacially adsorbed particle motion in a twofold way. On the one hand, the curvature gives rise to an effective potential well of gravitational energy that the particle experiences, that should be included in the force balance, on the other hand the curvature is causing inhomogeneities in the electric field, leading to dielectrophoretic forces in the lateral directions.

The pixels used in this study can be characterized by observing the voltage at which the oil film ruptures. This rupture voltage has been modeled and studied experimentally in reference [22]. The measured value of the rupture voltage is indicative of the interfacial tension and thickness dependence of the thin film capacitance of the pixel. In reference [22] the theoretical value for the rupture voltage is $V_c = C\left(\gamma/c''[h]L^2\right)^{1/2}$, with $c''[h]$ the second derivative of the thin film capacitance with respect to the oil film thickness. The dimensionless constant C depends on the mode of opening. For the lowest mode this constant is $C = 9.8$. In the SI the rupture voltage of a selection of pixels used in this study is measured. It is found that the rupture voltage varies between 45 and 68 V for a variety of initial curvatures and number of particles. One may expect that these parameters are of influence on the rupture voltage. However, the experimentally determined rupture voltages do not show a consistent trend with R_0. For a perfectly flat pixel in absence of particles the theoretical rupture voltage based on reference [22] is 85 V. This value is obtained for a surface tension of $\gamma = 0.051\,\mathrm{J/m^2}$, lateral pixel dimensions of 195x195 μm^2 and a pixel wall height of 10 μm. As can be seen, the calculated rupture voltage is higher than the largest value that is found experimentally. There are a few candidate explanations for this discrepancy. First, it cannot be excluded that the pixel wall material contains leachables that are potentially surface active and can lower the interfacial tension. A theoretical rupture voltage of 56 V can be obtained for a lower surface tension of 0.022 N/m. Another source of uncertainty is the point of pinning of the meniscus at the pixel wall. Since the edges are not sharp the point of pinning on the contact line is uncertain within a few μm. It is therefore more practical not to take the surface tension as the unknown but to consider the rupture voltage as the result of a lumped parameter $\left(\gamma/c''[h]\right)L^2)^{1/2}$ as described in [22].

As can be seen from the above considerations, the tilting method in present form is insufficient to measure the response of curvature to electric field. The primary reason being that the electric field is varying in the lateral direction due to curvature. This leads to dielectrophoretic forces exerted on the particle. These dielectrophoretic forces in turn influence the equilibrium position of the particle. Therefore, the tilting method in presence of an electric field measures the combined effect of the induced electrostatic forces on the particles and the change in curvature due to the electric field, details can be found in the SI. In the SI is explained that the change in curvature is reflected by the several terms present in the expression for a spring constant (see eqs. (16) and (17) in the SI). This gives an opportunity to measure the electrostatic forces, or equivalently, it's effective polarization, acting on the particle given the theoretically calculated response on the curvature presented in this work. In addition, a comprehensive methodology to characterize the curvature of the pixels has been established. This, in combination with the theoretical results from this paper, will enable to measure the electric field effects of interfacially adsorbed particles in more detail.

7. Conclusion

In this work we have demonstrated that electrowetting devices are excellent candidates to investigate electric field induced interactions between colloidal particles and may serve as a model for adjustable liquid lens arrays. In order to show this, initial curvatures have been quantified by measurement. Curvature radii were found to be ranging from 0.6-7 mm. In addition, fundamental calculations have been performed regarding the shape of the oil-water interface in such devices, with and without an electric field.

The deformation of a liquid-liquid interface by an applied electric field was calculated using a model invoking capillarity and electrostatics. Several factors that influence the curvature of the interface have been considered theoretically in this paper, these are: underfilling causing an initial curvature, fringe fields caused by the pixel wall and additional interfacially adsorbed colloidal particles. It has been found that the largest impact on the meniscus shape is given by the initial curvature. It is shown that the initial curvature can be maximally amplified when $V = V_c$. For values $V > V_c$ the interface is no longer stable. In the expression (24), the parameter β relates to the change in curvature as a result of an increase in the applied electric field. Based on the calculated value of $\beta = 0.76$ it is expected that the maximum amplification factor of the initial curvature is 1.76. Another useful result of the modeling is the relation between the oil film thickness and the curvature, see Eq. (14). This relation can be used to calculate the electric field strength in the center of the pixel, which is where possible added interfacially adsorbed particles are to be found. To correctly interpret experimental results that are conducted on such particles, a good estimate of this field strength is required.

These results could provide new opportunities in the fabrication and use of liquid lenses [27,28]. Furthermore, the experimental procedure of measuring the curvature and several model results give an opportunity to measure the electrostatic forces and capillary interactions of interfacially adsorbed particles [4,5,33,34].

CRediT authorship contribution statement

Faranaaz Rogier: Conceptualization, Investigation, Methodology, Visualization, Writing – review & editing. **Wan Shao:** Investigation. **Yuanyuan Guo:** Resources. **Lei Zhuang:** Software. **Willem K. Kegel:** Supervision, Writing – review & editing. **Jan Groenewold:** Conceptualization, Methodology, Software, Supervision, Writing – original draft.

Declaration of competing interest

The authors declare the following financial interests/personal relationships which may be considered as potential competing interests: Faranaaz Rogier reports financial support was provided by Dutch Research Council (TOPPUNT Grant).

Data availability

Data will be made available on request.

Appendix A. Supplementary material

Supplementary material related to this article can be found online at https://doi.org/10.1016/j.jcis.2023.11.099.

References

[1] A. Maestro, E. Guzmán, F. Ortega, R.G. Rubio, Contact angle of micro- and nanoparticles at fluid interfaces, Curr. Opin. Colloid Interface Sci. 19 (4) (2014) 355–367, https://doi.org/10.1016/j.cocis.2014.04.008, http://www.sciencedirect.com/science/article/pii/S1359029414000466.

[2] N. Ballard, A.D. Law, S.A. Bon, Colloidal particles at fluid interfaces: behaviour of isolated particles, Soft Matter 15 (6) (2019) 1186–1199, https://doi.org/10.1039/c8sm02048e.

[3] O.S. Deshmukh, D. Van Den Ende, M.C. Stuart, F. Mugele, M.H. Duits, Hard and soft colloids at fluid interfaces: adsorption, interactions, assembly & rheology, Adv. Colloid Interface Sci. 222 (2015) 215–227, https://doi.org/10.1016/j.cis.2014.09.003.

[4] P.A. Kralchevsky, K.D. Danov, N.D. Denkov, Capillary interactions between rough-edged particles, captive at a fluid interface, and rheology of particulate monolayers, Langmuir (2001) 7694–7705.

[5] G. Soligno, M. Dijkstra, R. Van Roij, Self-assembly of cubic colloidal particles at fluid-fluid interfaces by hexapolar capillary interactions, Soft Matter 14 (1) (2017) 42–60, https://doi.org/10.1039/c7sm01946g.

[6] I.B. Liu, N. Sharifi-Mood, K.J. Stebe, Capillary assembly of colloids: interactions on planar and curved interfaces, Annu. Rev. Condens. Matter Phys. 9 (1) (2018) 283–305, https://doi.org/10.1146/annurev-conmatphys-031016-025514, arXiv:1710.05258.

[7] P.A. Kralchevsky, K.D. Danov, P.V. Petkov, Soft electrostatic repulsion in particle monolayers at liquid interfaces: surface pressure and effect of aggregation, Philos. Trans. R. Soc. A, Math. Phys. Eng. Sci. 374 (2072) (2016), https://doi.org/10.1098/rsta.2015.0130.

[8] P. Pieranski, Two-dimensional interfacial colloidal crystals, Phys. Rev. Lett. 45 (7) (1980), https://doi.org/10.1103/PhysRevLett.45.569.

[9] a.J. Hurd, The electrostatic interaction between interfacial colloidal particles, J. Phys. A, Math. Gen. 18 (16) (1985) L1055–L1060, https://doi.org/10.1088/0305-4470/18/16/011.

[10] A. van Blaaderen, M. Dijkstra, R. van Roij, A. Imhof, M. Kamp, B.W. Kwaadgras, T. Vissers, B. Liu, Manipulating the self assembly of colloids in electric fields, Eur. Phys. J. Spec. Top. 222 (11) (2013) 2895–2909, https://doi.org/10.1140/epjst/e2013-02065-0.

[11] N. Aubry, P. Singh, Physics underlying controlled self-assembly of micro- and nanoparticles at a two-fluid interface using an electric field, Phys. Rev. E 77 (5) (2008) 056302, https://doi.org/10.1103/PhysRevE.77.056302, https://link.aps.org/doi/10.1103/PhysRevE.77.056302.

[12] M. Janjua, S. Nudurupati, P. Singh, N. Aubry, Electric field-induced self-assembly of micro- and nanoparticles of various shapes at two-fluid interfaces, Electrophoresis 32 (5) (2011) 518–526, https://doi.org/10.1002/elps.201000523.

[13] A.J. Pascall, T.M. Squires, Electrokinetics at liquid/liquid interfaces, J. Fluid Mech. 684 (2011) 163–191, https://doi.org/10.1017/jfm.2011.288.

[14] L. Chen, E. Bonaccurso, Electrowetting - from statics to dynamics, Adv. Colloid Interface Sci. 210 (2014) 2–12, https://doi.org/10.1016/j.cis.2013.09.007.

[15] J. Li, C.J. Kim, Current commercialization status of electrowetting-on-dielectric (EWOD) digital microfluidics, Lab Chip 20 (10) (2020) 1705–1712, https://doi.org/10.1039/d0lc00144a.

[16] M. Zhou, Q. Zhao, B. Tang, J. Groenewold, R.A. Hayes, G. Zhou, Simplified dynamical model for optical response of electrofluidic displays, Displays 49 (2017) 26–34, https://doi.org/10.1016/j.displa.2017.05.003.

[17] L. Ibarra-Bracamontes, M. Mossman, L. Whitehead, Characterization of large-scale interface deformation arising from electrostatic modification of the contact angle of pinned contact lines, J. Appl. Phys. 112 (6) (2012), https://doi.org/10.1063/1.4754426.

[18] A. Klingner, F. Mugele, Electrowetting-induced morphological transitions of fluid microstructures, J. Appl. Phys. 95 (5) (2004) 2918–2920, https://doi.org/10.1063/1.1643771.

[19] A. Bateni, S. Laughton, H. Tavana, S.S. Susnar, A. Amirfazli, A.W. Neumann, Effect of electric fields on contact angle and surface tension of drops, J. Colloid Interface Sci. 283 (1) (2005) 215–222, https://doi.org/10.1016/j.jcis.2004.08.134.

[20] G. Joffre, B. Prunet-Foch, S. Berthomme, M. Cloupeau, Deformation of liquid menisci under the action of an electric field, J. Electrost. 13 (2) (1982) 151–165, https://doi.org/10.1016/0304-3886(82)90005-5.

[21] R. Hayes, B. Feenstra, Video-speed electronic paper based on electrowetting, Nature 425 (2003), https://doi.org/10.1038/nature01988.

[22] B. Tang, J. Groenewold, M. Zhou, R.A. Hayes, G. Zhou, Interfacial electrofluidics in confined systems, Sci. Rep. 6 (May 2016) 1–7, https://doi.org/10.1038/srep26593.

[23] Q. Zhao, B. Tang, B. Dong, H. Li, R. Zhou, Y. Guo, Y. Dou, Y. Deng, J. Groenewold, A.V. Henzen, G. Zhou, Electrowetting on dielectric: experimental and model study of oil conductivity on rupture voltage, J. Phys. D, Appl. Phys. 51 (19) (2018), https://doi.org/10.1088/1361-6463/aabb69.

[24] B. Xu, Y. Guo, J. Barman, B.H. Erné, Y. Deng, G. Zhou, J. Groenewold, Impedance analysis of oil conductivity and pixel non-uniformity in electrowetting displays, Results Phys. 18 (2020), https://doi.org/10.1016/j.rinp.2020.103223.

[25] Y. Han, J. Koplik, C. Maldarelli, Surfactant and dilatational viscosity effects on the deformation of liquid droplets in an electric field, J. Colloid Interface Sci. 607 (2022) 900–911, https://doi.org/10.1016/j.jcis.2021.07.105.

[26] J. Chaudhuri, D. Bandyopadhyay, A coupled continuum-statistical model to predict interfacial deformation under an external field, J. Colloid Interface Sci. 587 (2021) 864–875, https://doi.org/10.1016/j.jcis.2020.11.047.

[27] B. Berge, Liquid lens technology: principle of electrowetting based lenses and applications to imaging, in: Proceedings of the IEEE International Conference on Micro Electro Mechanical Systems (MEMS), vol. 103, January 2005, 2005, pp. 227–230.

[28] L. Chen, M. Ghilardi, J.J. Busfield, F. Carpi, Electrically tunable lenses: a review, Front. Robot. AI 8 (June 2021) 1–20, https://doi.org/10.3389/frobt.2021.678046.

[29] A.L. Thorneywork, J.L. Abbott, D.G. Aarts, R.P. Dullens, Two-dimensional melting of colloidal hard spheres, Phys. Rev. Lett. 118 (15) (2017) 1–5, https://doi.org/10.1103/PhysRevLett.118.158001.

[30] Y. Guo, J. Yan, Z. Shen, H. Jiang, B. Tang, Y. Deng, A. Henzen, R. Zhou, G. Zhou, Electrofluidic displays based on inkjet printing and phase change filling, J. Micromech. Microeng. 30 (10) (2020), https://doi.org/10.1088/1361-6439/ab9e50.

[31] H. González, G. Néron de Surgy, J.-P. Chabrerie, Influence of bounded geometry on electrocapillary instability, Phys. Rev. B 50 (1994) 2520–2528, https://doi.org/10.1103/PhysRevB.50.2520, https://link.aps.org/doi/10.1103/PhysRevB.50.2520.

[32] H.A. Pohl, K. Pollock, J.S. Crane, Dielectrophoretic force: a comparison of theory and experiment, J. Biol. Phys. 6 (3–4) (1978) 133–160, https://doi.org/10.1007/BF02328936.

[33] K.D. Danov, P.A. Kralchevsky, Forces acting on dielectric colloidal spheres at a water/nonpolar fluid interface in an external electric field. 2. Charged particles, J. Colloid Interface Sci. 405 (2013) 269–277, https://doi.org/10.1016/j.jcis.2013.05.015.

[34] K.D. Danov, P.A. Kralchevsky, Forces acting on dielectric colloidal spheres at a water/nonpolar-fluid interface in an external electric field. 1. Uncharged particles, J. Colloid Interface Sci. 405 (2013) 278–290, https://doi.org/10.1016/j.jcis.2013.05.020.